AAC Accepted Manuscript Posted Online 19 October 2015
Antimicrob. Agents Chemother. doi:10.1128/AAC.01335-15

Structural basis of metallo-β-lactamase inhibition by captopril stereoisomers

Running title: Captopril stereoisomers and antibiotic resistance

Jürgen Brem[1*], Sander S. van Berkel[1*], David Zollman[1*], Sook Y. Lee[1], Opher Gileadi[2], Peter J. McHugh[3], Timothy R. Walsh[4], Michael A. McDonough[1#], and Christopher J. Schofield[1#]

[1] Department of Chemistry, University of Oxford, 12 Mansfield Road, Oxford, OX1 3TA, United Kingdom.

[2] Structural Genomics Consortium, University of Oxford, Old Road Campus, Headington, Oxford OX3 7BN, United Kingdom

[3] Department of Oncology, Weatherall Institute of Molecular Medicine, University of Oxford, John Radcliffe Hospital, Oxford OX3 9DS, United Kingdom.

[4] Department of Microbiology and Infectious Diseases, Institute of Infection and Immunity, Heath Hospital, Cardiff, CF14 4XN, United Kingdom.

* Co-first authors: Jürgen Brem, Sander S. van Berkel and David Zollman

[#] Corresponding Authors: Michael A. McDonough, Department of Chemistry, University of Oxford, 12 Mansfield Road, Oxford, OX1 3TA, United Kingdom, michael.mcdonough@chem.ox.ac.uk, and Christopher J. Schofield, Department of Chemistry, University of Oxford, 12 Mansfield Road, Oxford, OX1 3TA, United Kingdom, christopher.schofield@chem.ox.ac.uk

Abstract

β-Lactams are the most successful antibacterials, but their effectiveness is threatened by resistance, most importantly by production of serine- and metallo-β-lactamases (MBLs). MBLs are of increasing concern because they catalyse the hydrolysis of almost all β-lactam antibiotics, including recent generation carbapenems. Clinically useful serine-β-lactamase inhibitors have been developed, but such inhibitors are not available for MBLs. L-Captopril, used to treat hypertension via angiotensin-converting enzyme inhibition, has been reported to inhibit MBLs by chelating to the active site zinc ions *via* its thiol(ate). We report systematic studies on B1 MBL inhibition by all four captopril stereoisomers. High resolution crystal structures of three MBLs (IMP-1, BcII and VIM-2) in complex with either L-or D-captopril stereoisomers reveal correlations between the binding modes and inhibition potency. The results will be useful in the design of MBL inhibitors with the breadth of selectivity required for clinical application against carbapenem-resistant *Enterobacteriaceae* and other MBL mediated resistant infections.

37 **Introduction**

38 The increasing problem of antibiotic resistance is a global health concern (1), with the World
39 Health Organization (WHO) and the European Centre for Disease Prevention and Control
40 (ECDPC) reporting that several million people are infected with antibiotic resistant bacteria
41 annually. It is estimated that >50,000 patients die each year due to infections caused by
42 multidrug resistant bacterial pathogens in the United States of America alone (2).

43 β-Lactam containing compounds remain the most important antibiotics in clinical use, but
44 their effectiveness is threatened by increasing resistance. β-Lactam resistance is most
45 importantly mediated by serine- and zinc dependent metallo-β-lactamases (SBLs and MBLs,
46 respectively), which catalyse β-lactam hydrolysis (3). In combination with an appropriate
47 penicillin antibiotic, Class A SBL ('penicillinase') inhibitors (i.e. clavulanic acid,
48 tazobactam, and sulbactam) have been widely used in the clinic, and recently, a Class C
49 (cephalosporinase) SBL inhibitor (4), Avibactam, in combination with a cephalosporin has
50 been approved for clinical use (5). In contrast, there are no reports of clinically useful MBL
51 inhibitors (6).

52 A challenge with the development of useful MBL inhibitors is achieving the breadth of
53 inhibition against most MBL subtypes, whilst avoiding inhibition of structurally related
54 human MBL-fold enzymes (7). Crystal structures reveal that MBLs have a characteristic
55 αβ/βα sandwich fold, that they possess conserved zinc ion binding sites, and that loops
56 flanking the active site are involved in ligand binding (8). MBLs can be divided into three
57 subclasses (B1, B2 and B3) based on the number of zinc ions in their metal binding sites,
58 and/or sequence and structural similarities (6). B1 MBLs are the most clinically relevant
59 MBLs (e.g. IMP - Imipenemase, VIM - Verona integron–encoded MBL, and NDM - New
60 Delhi MBL types); B1 MBLs catalyse hydrolysis of almost all β-lactams (BLs), including the

latest generations of cephalosporins and carbapenems (9). Several classes of known metallo-enzyme inhibitors inhibit MBLs, including thiols, carboxylic acids, trifluoromethyl ketones, hydroxamic acids and rhodanines (7, 10, 11) (for structures see Figure S1 in the supplemental material).

(*2S*)-1-[(*2S*)-2-Methyl-3-sulfanylpropanoyl] pyrrolidine-2-carboxylic acid (commonly referred to as L-captopril) (Figure 1) is a thiol-containing small molecule which was developed in the 1970s to target the zinc-ion utilizing human angiotensin-converting enzyme (ACE) (12),(13). L-Captopril was successfully used for several decades to control high blood pressure. The clinically used (2*S*,2*S*)-stereoisomer of captopril, i.e. L-captopril inhibits several MBLs from all subclasses (14-18). However, the (2*S*,2*R*)-stereoisomer, (*2S*)-1-[(*2R*)-2-methyl-3-sulfanylpropanoyl] pyrrolidine-2-carboxylic acid (Figure 1), commonly referred to as D-captopril, has been reported to be more active than L-captopril against some MBLs (e.g. NDM-1 (19), BcII (17), CcrA (20) and CphA (17)).

Crystal structures have been reported for some MBLs in complex with L- or D-captopril, i.e. (i) in the case of the B1 subclass MBLs, for NDM-1 complexed with L-captopril (21) and BlaB (*Chryseobacterium meningosepticum*) with D-captopril (22); (ii) in the case of the B2 MBLs, for CphA (*Aeromonas hydrophilia*) with D-captopril (18); and (iii) in the case of the B3 MBLs, for FEZ-1 (*Fluoribacter gormanii* MBL) with D-captopril (23) and L1 (*Stenotrophomonas maltophilia* MBL) with D-captopril (15). Biophysical analyses employing extended X-ray absorption fine structure (EXAFS), and perturbed angular correlation of X-rays (PAC) spectroscopy have been reported for BcII and CphA complexed with D- and L-captopril (17). Molecular dynamic calculations on D- and L-captopril complexed with BcII and D-captopril with NDM-1 have also been reported (20, 24). These analyses imply that both L- and D-captopril can bind with their thiol(ate) ligated to both active site Zn(II) ions (Figure 2; see Figure S2-4 and 2D diagram in the supplemental material). Interestingly,

86 despite BlaB and NDM-1 belonging to the same B1 MBL subclass, different binding modes
87 were observed for the L- and D-captopril stereoisomers (19). In the case of the mono-Zn(II)
88 ion binding B2 subclass a structure of the CphA:D-captopril complex (18) indicates that the
89 D-captopril carboxylate, rather than the thiol(ate), binds to the single Zn(II) ion, a binding
90 mode that possibly reflects the relatively weak inhibition of this enzyme by D-captopril (K_i =
91 72 μM). Finally, with the B3 MBL subclass, in a crystal structure of the FEZ-1:D-captopril
92 complex (23) the binding of captopril was modelled such that neither the D-captopril thiol nor
93 carboxylate interacts with the active site Zn(II) ions, a binding mode that was also proposed
94 to be consistent with the relatively weak inhibition observed in this case (K_i 400 μM) (see
95 Figure S2 in the supplemental material). To date there have been no reports on MBL
96 inhibition by (2*R*)-1-[(2*S*)-2-methyl-3-sulfanylpropanoyl] pyrrolidine-2-carboxylic acid,
97 subsequently referred to as *epi*-L-captopril (the 2*R*,2*S*-stereoisomer) and (2*R*)-1-[(2*R*)-2-
98 methyl-3-sulfanylpropanoyl] pyrrolidine-2-carboxylic acid, subsequently referred to as *epi*-D-
99 captopril (the 2*R*,2*R*-stereoisomer) (Figure 1).
100 We report systematic studies on the inhibition of four clinically relevant MBLs (IMP-1, VIM-
101 2, SPM-1 and NDM-1) and the model MBL, BcII, by the four captopril stereoisomers and
102 both enantiomers of a captopril derivative 1-(2-mercaptobenzoyl)pyrrolidine-2-carboxylic
103 acid (D- and L-MBP) (Figures 1 and Table S1 in the supplemental material) (25, 26). The
104 combined kinetic and structural studies clearly reveal different binding modes for different
105 captopril stereoisomers, and will help to enable the future development of broad spectrum
106 MBL inhibitors.
107

Materials and methods

Synthesis

The different captopril isomers and captopril derivatives were prepared according to literature procedures (see Scheme S1 and S2 and the experimental section in the supplemental material).

Protein production and purification

Recombinant forms of NDM-1, VIM-2, VIM-4, SPM-1, IMP-1 and BcII MBLs were produced in *Escherichia coli* as described (27, 28). Purified proteins were dialysed into freshly prepared crystallisation buffer (50 mM HEPES pH 7.5, 150 mM NaCl containing 1 µg $ZnCl_2$) then concentrated [to 2 mM (BcII), 0.75 mM (IMP-1) and 0.36 mM (VIM-2)] before use in crystallisation studies.

Crystallography

Crystals were grown using the conditions stated in Table S2 in the supplemental material, and cryoprotected using well solution diluted with 25% glycerol before being flash cooled in liquid nitrogen. All data sets were collected at 100K. All data were indexed, integrated and scaled using HKL-3000 (29). The structures were solved by molecular replacement using Phaser (30). The structures were then refined using PHENIX (31) and COOT (32) until R_{work} and R_{free} no longer decreased. Data collection and refinement statistics are given in Table S3-5 in the supplemental material.

Coordinates and structure factors have been deposited with PDB accession codes: di-Zn(II)-BcII *apo* (PDB ID: 4C09), BcII L-captopril (PDB ID: 4C1H), BcII D-captopril (PDB ID: 4C1C), IMP-1 L-captopril (PDB ID: 4C1F), IMP-1 D-captopril (PDB ID: 4C1G), di-Zn(II)-

131 VIM-2 *apo* (PDB ID: 4BZ3), VIM-2 L-captopril (PDB ID: 4C1D), VIM-2 D-captopril (PDB
132 ID: 4C1E). The URL for coordinate deposition is **http://rcsb-deposit.rutgers.edu/**.

133 **Kinetic analyses**

134 Kinetic and inhibition assays with the bacterial MBLs, *h*ACE-2 (Angiotensin-converting
135 enzyme 2) and *h*HAGH (Hydroxyacylglutathione hydrolase, human Glyoxylase II were
136 performed as described (7, 27).

137 **Nuclease assays**

138 Nuclease assays with DCLRE1A and DCLRE1B (DNA cross-link repair enzymes 1A and B)
139 (33) used the described method (33) employing a 21-nucleotide DNA oligonucleotide with a
140 fluorescein label at its 3'-end. In brief, exonuclease activity was measured using ΔN-
141 DCLRE1A (3.5 ng, 8 nM) or ΔC-DCLRE1B (1.5 ng, 4 nM) mixed with 1 pmol (1 μM) of 3′
142 fluorescein-labeled DNA substrate in 10 μL of 20 mM HEPES pH 7.9, 50 mM KCl, 10 mM
143 $MgCl_2$, 0.5 mM DTT, 0.05 % Triton-X, 0.1 mg/mL BSA and 5 % glycerol. Reactions were
144 incubated at 37 °C for 20 minutes with the indicated concentrations of D-captopril, L-
145 captopril, D-MBP, or L-MBP (see Figure S5 in the supplemental material) and quenched by
146 addition of 2 μL of 80 % formamide/ 10 mM EDTA and heating at 95 °C for 5 min.
147 Following separation on a 20 % polyacrylamide/ 7 M urea denaturing gel, substrate and
148 product bands were visualised by a Typoon Trio+ Variable Model Imager (excitation at 488
149 nm with blue laser at 400 V).

150 **MIC determinations**

151 The bacteria used were non-clonal international isolates where the mechanisms of
152 carbapenem resistance have been genetically defined by sequencing. As a negative control *E.*
153 *coli* ATCC 25922 was used. MBL genes were obtained by PCR using standard procedures

154 and inserted into a pK18 vector which was used to transform *E. coli* J53(34). Transconjugates
155 were MBL genes carried on native wild-type plasmids conjugated into J53 (35). Both
156 transformants and transconjugants were verified by DNA sequencing and for MBL
157 production by using the MTS MBL strip (Liofilchem, Roseto, Italy). Additionally, five
158 *Escherichia coli* (NDM-1), 10 *Klebsiella pneumoniae* (5 NDM-1, 3 VIM-4 and 2 IMP-4),
159 one *Serratia macescens* (IMP-4), two *Pseudomonas aeruginosa* (VIM-2, AIM-1) and *E. coli*
160 ATCC 25922 were used in the test panel. MICs were determined using microbroth dilution
161 method according to CLSI guidelines. Strains were cultured and tested in cation adjusted
162 Muller-Hinton agar and broth (Beckton Dickinson, USA).
163

Results

MBL inhibition by Captopril stereoisomers

We first synthesised the four possible captopril stereoisomers (D-, L-, *epi*-D- and *epi*-L-captopril, see Scheme S1 and S2 and Experimental section in the supplemental material) and tested them as inhibitors against BcII and clinically relevant MBLs from the B1 subclass (IMP-1, VIM-2, SPM-1 and NDM-1) (Table 1 and Figure 3) (9). Comparing the previously reported D-captopril and L-captopril inhibition values to our results for NDM-1, IMP-1 and BcII reveals relatively small differences (Table 1), likely due, at least in part, to different assay conditions (for D-captopril: NDM-1 IC_{50} 20.1 μM vs 7.9 μM (36); BcII IC_{50} 10.7 μM vs 45 μM (K_i) (17) and for L-captopril: NDM-1 IC_{50} 157.4 μM vs 202 μM (36); IMP-1 IC_{50} 7.2 μM vs 12.5 μM (K_i) (37) and BcII IC_{50} 80.4 μM vs 65 μM (K_i) (17)). In all cases D-captopril was the most potent of the four possible captopril stereoisomers (NDM-1 IC_{50} 20.1±1.5 μM, IMP-1 IC_{50} 7.2±1.2 μM, VIM-2 IC_{50} 0.072±0.010 μM, SPM-1 IC_{50} 261.8±1.3 μM and BcII IC_{50} 10.7±1.2 μM) (Table 1). D-Captopril was consistently more potent than L-captopril (~7 fold for NDM-1, ~3 fold for IMP-1, ~60 fold for VIM-2, ~2 fold for SPM-1 and ~8 fold for BcII) (Table 1). Both *epi*-L- and *epi*-D-captopril were poor inhibitors of BcII and SPM-1 (IC_{50} values all ≥ 500 μM); whereas for NDM-1 and IMP-1, unlike *epi*-L-captopril, *epi*-D-captopril showed some activity (NDM-1 IC_{50} 64 μM and IMP-1 IC_{50} 173 μM). Relatively potent IC_{50} values were observed for both *epi*-L- and *epi*-D-captopril against VIM-2 (IC_{50} 5.5 μM). The captopril derivatives, D- and L-MBP, were less potent (IC_{50} > 500 μM) against all MBLs when compared to D- and L-captopril (Table 1).

A key issue in work towards obtaining clinically relevant MBL inhibitors is the degree of selectivity of the bacterial MBLs over that of human metallo-enzymes, including MBL-fold enzymes. Although L-captopril is a well-studied ACE-2 inhibitor, there are no reports of its selectivity versus human-MBL-fold enzymes. We tested L- and D-captopril, as well as D- and

L-MBP against the human MBL fold enzymes DCLRE1A and DCLRE1B (33), *h*HAGH and *h*ACE-2 (zinc dependent human metallo enzyme); no inhibition was observed at 100 μM under our standard assay conditions (see Figure S5 in the supplemental material).

Pathogen susceptibility to D – and L-captopril

Since D- and L-captopril captopril were consistently the most potent stereoisomers against the tested MBLs (Table 2), we tested them against non-clonal multidrug-resistant bacteria expressing various MBLs. We used a variety of cloned MBLs, conjugant, and wild-type clinical isolates. The panel of strains were tested for meropenem/ceftazidime MICs with and without L- or D-captopril at 8 mg/L. (Table 2). In order to correlate with the cellular studies (see below), we determined the IC_{50} values for D-and L-captopril against VIM-4 (VIM-4 IC_{50} 1.7±0.4 μM for D-captopril and IC_{50} 3.9±0.5 μM for L-captoril). Pathogenic strains from different geographical origins (e.g. Greece (A-33, VIM-4) or India (IR 60, NDM-1)) (38), and display resistance against BLs as well as fluoroquinoline and aminoglycoside antibiotics were selected for MIC tests (Table 2). Whilst L-captopril showed potentiation with cloned and transconjugated MBLs, against wild-type strains there was little synergy observed and generally less than D-captopril (Table 2). The addition of D-captopril potentiates the efficacy of meropenem against most of the VIM-2, VIM-4, IMP-4 and NDM-1 producing strains tested including *E. coli*, *K. pneumoniae*, *S. marascens*, and *P. aeruginosa* (Table 2).

Structural analysis of captopril binding to IMP-1, VIM-2 and BcII

We then investigated the mode of binding of the captopril stereoisomers to MBLs by crystallography. We determined high-resolution crystal structures for D- or L-captopril in complex with IMP-1 (1.71 and 2.01 Å resolution, respectively), VIM-2 (1.40 and 1.20 Å resolution, respectively) and BcII (1.18 and 1.10 Å resolution, respectively). For comparison, structures of di-Zn(II)-VIM-2 and di-Zn(II)-BcII without inhibitors were also determined, to

214 1.20 and 1.30 Å resolution, respectively. For all structures, the 'crystal systems' were similar
215 to those previously reported (VIM-2 (7), IMP-1 (39) and BcII (40)). (Note, we use the
216 standard numbering scheme for class B β-lactamases (BBL numbering (41)).
217 As anticipated, in all cases the overall protein folds observed were the characteristic αβ/βα
218 MBL sandwich fold (2 β-sheets sandwiched with 2 helices buttressed against each external
219 face of the sandwich) (8). The active sites, which are located at one end of the two β-sheets in
220 a groove surrounded by several loops, were in all cases occupied by two zinc ions as
221 expected for B1 subclass MBLs. The L3 and L10 loops which flank the active site are located
222 opposite each other and are involved in substrate binding (42). The L3 loop (residues 61–66
223 (BBL numbering)) is located between strands β3 and β4 and the L10 loop (residues 223–241)
224 is located between strand β11 and helix α4, which includes Lys224/Arg228 and Asn233, the
225 side chains of which are directly involved in substrate and inhibitor binding (41, 43).
226 The electron density maps for the ligands in the various MBL:captopril complexes suggested
227 variable ligand occupancies and were carefully analysed between rounds of refinement (see
228 example Figure S6 in the supplemental material). For BcII, both D- and L-captopril were
229 modelled and refined with 70% occupancy. For the VIM-2:D-captopril complex structure, the
230 ligands were modelled and refined with 100% occupancy and for the VIM-2:L-captopril
231 complex with 80% occupancy. In the IMP-1:D-captopril and IMP-1:L-captopril structures the
232 ligands were modelled and refined with 100% occupancy in chain A, but the residual density
233 present in chain B was interpreted as too weak (< 50% occupancy) to include in the model.
234 Preliminary structural analysis indicated partial oxidation of the metal binding cysteine
235 (Cys221) had occurred in both the crystallised BcII and VIM-2 proteins, in similar manner to
236 that observed in previous crystallographic studies on these B1 MBLs (40, 44). Due to the
237 likelihood of active site cysteine oxidation (Cys221) interfering with the active site Zn(II)
238 chemistry and hence with our analysis of ligand binding, we worked to minimise Cys221

239 oxidation. In all cases, cysteine oxidation during crystallisation could be prevented by the
240 addition of tris(2-carboxyethyl)phosphine (TCEP) (40) (except for IMP-1 where cysteine
241 oxidation in the absence of TCEP was not observed).

242 Our MBL:captopril complex structures show a similar overall captopril binding mode to
243 those previously observed for NDM-1:L-captopril (21), BlaB:D-captopril (22) and L1:D-
244 captopril (15), but differ significantly from the FEZ-1:D-captopril (23) and CphA: D-captopril
245 complex structures (Figure 3; see Figure S2 in the supplemental material). Our MBL:L-
246 captopril structures are most similar to the reported NDM-1:L-captopril complex structure
247 (21) and our MBL:D-captopril structures are most similar to the L1:D-captopril complex
248 structure (15) (see Figure S2 in the supplemental material). Comparison of the MBL:captopril
249 complex structures with the active site of apo-MBLs reveals that several water molecules are
250 displaced upon the binding of the D- or L-captopril (see Figure S7 in the supplemental
251 material), these displacements likely contribute to the strength of inhibitor binding.

252 Captopril has distinct features that enable metallo-protein binding. The thiol acts as a metal
253 binding ligand that displaces the proposed 'hydrolytic' water molecule (or hydroxide) that
254 bridges the two active site metal ions. A carbonyl group leads to the conformationally
255 constrained prolyl-ring and a methyl group extends from the carbon bonded to the thiol. Both
256 the L- and D-captopril diastereoisomers present two distinct binding faces (Figure 4). One
257 face is hydrophobic and is formed by the methyl group and the proline ring methylenes; the
258 hydrophobic face interacts with residues from the L3 loop ($Trp87_{BcII}$; $Trp64_{IMP-1}$ and
259 $Val61_{IMP-1}$; and $Trp87_{VIM-2}$, $Phe61_{VIM-2}$ and $Tyr67_{VIM-2}$) (Figure 4). Such interactions are in
260 agreement with the proposed role of the 'mobile' L3 loop in interacting with the hydrophobic
261 *N*-acyl substituents of cephalosporin and penicillin MBL substrates (45). The other face of
262 captopril is more hydrophilic and is positioned to form hydrogen bonds to residues in the L10
263 loop. In all our MBL:D-captopril structures, the D-captopril carboxylate is positioned to form

264 electrostatic and hydrogen-bonding interactions distances ranging from 2.9 Å for BcII and
265 VIM-2 to 2.3 Å for IMP-1 with a conserved positively charged residue ($Lys224_{IMP-1,BcII}$ or
266 $Arg228_{VIM-2}$), which is predicted to be involved in binding the β-lactam substrate carboxylate
267 (46, 47) (Figure 4 and Figure S4 in the supplemental material). As observed for our MBL:D-
268 captopril structures, the IMP-1:L-captopril structure also has the inhibitor carboxylate
269 positioned to form an electrostatic interaction with the conserved basic residue, i.e. Lys224.
270 In contrast, in the BcII:L-captopril and VIM-2:L-captopril structures, the captopril
271 carboxylate is orientated away from the conserved positively charged Lys/Arg residue
272 (Lys224/Arg228). In all MBL:L-captopril structures (including for IMP-1), the carboxylate is
273 positioned to interact with the conserved asparagines (Asn233) from the L10 loop. IMP-1 is
274 thus apparently special case, i.e. where both L- and D-captopril bind in similar modes with the
275 inhibitor carboxylate positioned to interact with $Lys224_{IMP-1}$. In the structures of BcII and
276 VIM-2 complexed with D-captopril and of VIM-2 with L-captopril, the captopril amide
277 carbonyl oxygen is positioned to interact with the conserved asparagine (Asn233) from the
278 L10 loop (Figure 4 and see Figure S4 in the supplemental material). In all cases the L3 and
279 L10 loops were observed to move slightly towards the inhibitors relative to their positions in
280 the absence of inhibitor, consistent with an induced fit mechanism during substrate binding.
281 This is most clearly observed in the case of VIM-2 (Figure 4).
282 The observed binding modes for the D-captopril carboxylate in our structures differ from the
283 binding mode observed in the reported BlaB D-captopril structure (22) despite a similar
284 binding mode of the captopril thiol(ate) to the zinc ions. In the case of BlaB the D-captopril
285 carboxylate is rotated by ~180,° elative to the thiolate mode of binding in our structures, such
286 that it does not interact with the conserved $Lys224_{BlaB}$, but binds to $Lys167_{BlaB}$ from the L10
287 loop. The conserved $Asn233_{BBL}$ in the L10 loop is replaced by tyrosine in BlaB (22); this
288 Asn-Tyr substitution likely contributes to the different D-captopril binding mode in BlaB

289 compared to our structures. Thus, D-captopril is likely to bind to NDM-1, which contains an
290 asparagine ($Asn233_{BBL}$) rather than a tyrosine at this position, in a similar manner to that
291 observed for BcII, IMP-1, and VIM-2 (rather than the BlaB binding mode) (21).
292 In all of our MBL:captopril structures, the distance from the Zn(II) atoms to the bridging
293 thiolate sulphur atom is ~2.3 Å. Similar distances are reported for the BlaB (B1) and L1 (B3)
294 D-captopril structures (PDB IDs: 1M2X and 2FU8) with a slightly smaller distance for the L-
295 captopril NDM-1 structure (PDB ID: 4EXS) (21). Different values have been observed for
296 the MBL inter-metal distance in the absence of exogenous ligands, with reported values
297 ranging from 2.5 to 4.5 Å (48), which may in part be dependent on the actual metals bound,
298 which is not always possible to assign based on diffraction data alone (48). An inter-zinc
299 distance of 3.5 Å was observed for both our di-Zn(II)-BcII and di-Zn(II)-VIM-2 apo
300 structures, where, as previously observed, a bridging water was present. The inter-zinc
301 distances increase to 3.8 Å and 3.7 Å upon D- or L-captopril binding to BcII and VIM-2,
302 respectively, with the binding thiolate. This observation is consistent with the different van
303 der Waals atomic radii for sulphur (1.8 Å) and oxygen (1.5 Å). For IMP-1 the observed Zn-
304 Zn distance (3.5 Å (PDB ID: 1DDK) (39), as in our BcII and VIM-2 structures) increased to
305 3.7 Å on binding of either the L- or D-captopril stereoisomers.
306

307 **Discussion**

308

309 Although once of little clinical relevance, MBLs are now of increasing importance (6). The
310 VIM type B1 MBLs are a major problem in parts of Asia, being present in up to 99% of MBL
311 positive multidrug resistant strains (49). Thus, there is a genuine need for a response to MBL-
312 mediated resistance. The finding that D-captopril, a stereoisomer of the clinically used L-
313 captopril, is consistently the most potent inhibitor of the captopril stereoisomers against
314 MBLs and can potentiate meropenem against VIM-2 and other MBL expressing pathogens is
315 of interest.

316 Although several crystal structures of MBLs in combination with either D- or L-captopril
317 have been reported, structures of the same MBL in complex with D- and L-captopril isomers
318 have not been reported previously. The captopril isomer binding modes that we observe are
319 related in that they all involve thiol(ate) zinc chelation, as in most of the previously reported
320 structures. An exception is the reported FEZ-1:D-captopril structure (23), which, due to its
321 relatively poor quality, may not be representative of binding in solution.

322 Correlations between the observed binding modes and the potency of inhibition can be made.
323 More potent inhibition was always observed when an interaction between the captopril
324 carboxylate and the conserved basic Lys/Arg ($Lys224_{BBL}$) involved in substrate binding is
325 observed in the crystal structures. In all cases, VIM-2 manifested lower IC_{50} values compared
326 to the other tested MBLs - this correlates with the additional interactions observed between
327 $Arg228_{VIM-2}$ with the captopril carboxylate, as well as additional interactions of the VIM-2 L3
328 loop with the hydrophobic face of captopril. Secondly, the observation of a decreased number
329 of hydrogen bonding/electrostatic interactions for L- over D-captopril generally reflects
330 weaker inhibition. L-Captopril was observed to be more potent in the case of IMP-1 than for
331 the other MBLs tested and its IC_{50} value was only 3-fold higher than D-captopril. This
332 observation of relative potent inhibition for IMP-1 by L- captopril correlates with the

333 observation that for IMP-1, but none of the other MBLs, the L-captopril carboxylate favours
334 binding to $Lys224_{IMP-1}$.

335 Product inhibition is commonly observed for MBLs (16). Comparison of our MBL:captopril
336 structural complexes with the MBL:β-lactam product complexes (PDB ID: 4HL2) (Figure 1),
337 shows that the most potent of the captopril isomers, D-captopril, has the most similar mode of
338 binding to hydrolysed β-lactams (50), especially penicillins, consistent with D-captopril being
339 the most potent inhibitor (Table 1). However, D-captopril was significantly less potent (> 20
340 fold) against SPM-1 than for all other MBLs tested; the other captopril stereoisomers did not
341 inhibit SPM-1 (IC_{50} > 500 μM). This difference may reflect the unusual nature of SPM-1 as a
342 proposed B1/B2 'hybrid' MBL.(42) A challenge in MBL inhibition is to obtain the breadth of
343 selectivity towards the majority of prokaryotic MBLs, often with relatively low sequence
344 similarity (~30% for the MBLs we used) (see Table S1 in the supplemental material), without
345 inhibiting the related human MBL-fold enzymes. The combined structural and inhibition
346 results reveal that captopril stereoisomers can potently inhibit B1 MBLs via related, but
347 sometimes different binding modes. These observations may be important in developing
348 potent inhibitors with the required breadth of selectivity against different subtypes of MBLs,
349 i.e. medicinal chemists may specifically aim to identify single compounds that bind
350 differently to different MBL subtypes.

351

352 **Acknowledgements**

353 We thank the Medical Research Council (MRC)/Canadian Grant G1100135 and
354 MR/L007665/1 grant for support of J.B, S.Y.B, P.J.M and C.J.S. Cancer Research UK
355 (CRUK) is kindly acknowledged for the support of S.S.v.B and C.J.S and the Biotechnology
356 and Biological Sciences Research Council (BBSRC) for the support of C.J.S.

357 **References**

358 1. **Berendonk TU, Manaia CM, Merlin C, Fatta-Kassinos D, Cytryn E, Walsh F, Burgmann H,**
359 **Sorum H, Norstrom M, Pons M-N, Kreuzinger N, Huovinen P, Stefani S, Schwartz T, Kisand**
360 **V, Baquero F, Martinez JL.** 2015. Tackling antibiotic resistance: the environmental
361 framework. Nat Rev Micro **13:**310-317.

362 2. **No authors listed.** 2013. The antibiotic alarm. Nature **495:**141.

363 3. **Bush K.** 2013. Proliferation and significance of clinically relevant β-lactamases. Ann N Y Acad
364 Sci **1277:**84-90.

365 4. **Bebrone C, Lassaux P, Vercheval L, Sohier JS, Jehaes A, Sauvage E, Galleni M.** 2010. Current
366 challenges in antimicrobial chemotherapy: focus on ss-lactamase inhibition. Drugs **70:**651-
367 679.

368 5. **Ehmann DE, Jahić H, Ross PL, Gu RF, Hu J, Durand-Réville TF, Lahiri S, Thresher J, Livchak S,**
369 **Gao N, Palmer T, Walkup GK, Fisher SL.** 2013. Kinetics of avibactam inhibition against class
370 A, C, and D β-lactamases. J Biol Chem **288:**27960-27971.

371 6. **Cornaglia G, Giamarellou H, Rossolini GM.** 2011. Metallo-β-lactamases: a last frontier for β-
372 lactams? Lancet Infect Dis **11:**381-393.

373 7. **Brem J, van Berkel SS, Aik W, Rydzik AM, Avison MB, Pettinati I, Umland KD, Kawamura A,**
374 **Spencer J, Claridge TD, McDonough MA, Schofield CJ.** 2014. Rhodanine hydrolysis leads to
375 potent thioenolate mediated metallo-β-lactamase inhibition. Nat Chem **6:**1084-1090.

376 8. **Carfi A, Pares S, Duee E, Galleni M, Duez C, Frère JM, Dideberg O.** 1995. The 3-D structure
377 of a zinc metallo-β-lactamase from Bacillus cereus reveals a new type of protein fold. Embo j
378 **14:**4914-4921.

379 9. **Karsisiotis AI, Damblon CF, Roberts GCK.** 2014. A variety of roles for versatile zinc in
380 metallo-β-lactamases. Metallomics **6:**1181-1197.

381 10. **Fast W, Sutton LD.** 2013. Metallo-β-lactamase: inhibitors and reporter substrates. Biochim
382 Biophys Acta **1834:**1648-1659.

383 11. **Buynak JD.** 2013. β-Lactamase inhibitors: a review of the patent literature (2010 - 2013).
384 Expert Opin Ther Pat **23:**1469-1481.

385 12. **Li N, Xu Y, Xia Q, Bai C, Wang T, Wang L, He D, Xie N, Li L, Wang J, Zhou HG, Xu F, Yang C,**
386 **Zhang Q, Yin Z, Guo Y, Chen Y.** 2014. Simplified captopril analogues as NDM-1 inhibitors.
387 Bioorg Med Chem Lett **24:**386-389.

388 13. **Day JA, Cohen SM.** 2013. Investigating the selectivity of metalloenzyme inhibitors. J Med
389 Chem **56:**7997-8007.

390 14. **Ma J, Cao Q, McLeod SM, Ferguson K, Gao N, Breeze AL, Hu J.** 2015. Target-Based Whole-
391 Cell Screening by ^{1}H NMR Spectroscopy. Angew Chem Int Ed Engl **54:**4764-4767.

392 15. **Nauton L, Kahn R, Garau G, Hernandez JF, Dideberg O.** 2008. Structural insights into the
393 design of inhibitors for the L1 metallo-β-lactamase from Stenotrophomonas maltophilia. J
394 Mol Biol **375:**257-269.

395 16. **Badarau A, Page MI.** 2006. The variation of catalytic efficiency of Bacillus cereus metallo-β-
396 lactamase with different active site metal ions. Biochemistry **45:**10654-10666.

397 17. **Heinz U, Bauer R, Wommer S, Meyer-Klaucke W, Papamichaels C, Bateson J, Adolph HW.**
398 2003. Coordination geometries of metal ions in D- or L-captopril-inhibited metallo-β-
399 lactamases. J Biol Chem **278:**20659-20666.

400 18. **Lienard BM, Garau G, Horsfall L, Karsisiotis AI, Damblon C, Lassaux P, Papamicael C,**
401 **Roberts GC, Galleni M, Dideberg O, Frère JM, Schofield CJ.** 2008. Structural basis for the
402 broad-spectrum inhibition of metallo-β-lactamases by thiols. Org Biomol Chem **6:**2282-2294.

403 19. **Rydzik AM, Brem J, van Berkel SS, Pfeffer I, Makena A, Claridge TD, Schofield CJ.** 2014.
404 Monitoring conformational changes in the NDM-1 metallo-β-lactamase by ^{19}F NMR
405 spectroscopy. Angew Chem Int Ed Engl **53:**3129-3133.

406 20. **Antony J, Gresh N, Olsen L, Hemmingsen L, Schofield CJ, Bauer R.** 2002. Binding of D- and L-
407 captopril inhibitors to metallo-β-lactamase studied by polarizable molecular mechanics and
408 quantum mechanics. J Comput Chem **23:**1281-1296.

409 21. **King DT, Worrall LJ, Gruninger R, Strynadka NC.** 2012. New Delhi metallo-β-lactamase:
410 structural insights into β-lactam recognition and inhibition. J Am Chem Soc **134:**11362-
411 11365.

412 22. **Garcia-Saez I, Hopkins J, Papamicael C, Franceschini N, Amicosante G, Rossolini GM,**
413 **Galleni M, Frère JM, Dideberg O.** 2003. The 1.5-A structure of Chryseobacterium
414 meningosepticum zinc β-lactamase in complex with the inhibitor, D-captopril. J Biol Chem
415 **278:**23868-23873.

416 23. **Garcia-Saez I, Mercuri PS, Papamicael C, Kahn R, Frère JM, Galleni M, Rossolini GM,**
417 **Dideberg O.** 2003. Three-dimensional structure of FEZ-1, a monomeric subclass B3 metallo-
418 β-lactamase from Fluoribacter gormanii, in native form and in complex with D-captopril. J
419 Mol Biol **325:**651-660.

420 24. **Wang YT, Chi-Yu L.** 2014. Inhibitor and Substrate Binding by New Delhi metallo-β-lactamase-
421 1: A Molecular Dynamics Studies. Curr Comput Aided Drug Des.

422 25. **Menard PR, Suh JT, Jones H, Loev B, Neiss ES, Wilde J, Schwab A, Mann WS.** 1985.
423 Angiotensin converting enzyme inhibitors. (Mercaptoaroyl)amino acids. J Med Chem **28:**328-
424 332.

425 26. **Skiles JW, Suh JT, Williams BE, Menard PR, Barton JN, Loev B, Jones H, Neiss ES, Schwab A.**
426 1986. Angiotensin-converting enzyme inhibitors: new orally active 1,4-thiazepine-2,5-diones,
427 1,4-thiazine-2,5-diones, and 1,4-benzothiazepine-2,5-diones possessing antihypertensive
428 activity. J Med Chem **29:**784-796.

Antimicrobial Agents and Chemotherapy

429 27. **van Berkel SS, Brem J, Rydzik AM, Salimraj R, Cain R, Verma A, Owens RJ, Fishwick CWG,**
430 **Spencer J, Schofield CJ.** 2013. Assay Platform for Clinically Relevant Metallo-β-lactamases. J
431 Med Chem **56:**6945-6953.

432 28. **Lassaux P, Traore DA, Loisel E, Favier A, Docquier JD, Sohier JS, Laurent C, Bebrone C, Frere**
433 **JM, Ferrer JL, Galleni M.** 2011. Biochemical and structural characterization of the subclass
434 B1 metallo-β-lactamase VIM-4. Antimicrob Agents Chemother **55:**1248-1255.

435 29. **Otwinowski Z, Minor W.** 1997. Processing of X-ray diffraction data collected in oscillation
436 mode, p 307-326, vol 276. Elsevier.

437 30. **McCoy AJ, Grosse-Kunstleve RW, Adams PD, Winn MD, Storoni LC, Read RJ.** 2007. Phaser
438 crystallographic software. J Appl Crystallogr **40:**658-674.

439 31. **Adams PD, Afonine PV, Bunkoczi G, Chen VB, Davis IW, Echols N, Headd JJ, Hung LW,**
440 **Kapral GJ, Grosse-Kunstleve RW, McCoy AJ, Moriarty NW, Oeffner R, Read RJ, Richardson**
441 **DC, Richardson JS, Terwilliger TC, Zwart PH.** 2010. PHENIX: a comprehensive Python-based
442 system for macromolecular structure solution. Acta Crystallogr D Biol Crystallogr **66:**213-
443 221.

444 32. **Emsley P, Lohkamp B, Scott WG, Cowtan K.** 2010. Features and development of Coot. Acta
445 Crystallogr D Biol Crystallogr **66:**486-501.

446 33. **Sengerová B, Allerston CK, Abu M, Lee SY, Hartley J, Kiakos K, Schofield CJ, Hartley JA,**
447 **Gileadi O, McHugh PJ.** 2012. Characterization of the human SNM1A and SNM1B/Apollo DNA
448 repair exonucleases. Journal of Biological Chemistry **287:**26254-26267.

449 34. **Yong D, Toleman MA, Giske CG, Cho HS, Sundman K, Lee K, Walsh TR.** 2009.
450 Characterization of a new metallo-β-lactamase gene, bla(NDM-1), and a novel erythromycin
451 esterase gene carried on a unique genetic structure in Klebsiella pneumoniae sequence type
452 14 from India. Antimicrob Agents Chemother **53:**5046-5054.

Antimicrobial Agents and Chemotherapy

453 35. **El Salabi A, Borra PS, Toleman MA, Samuelsen O, Walsh TR.** 2012. Genetic and biochemical
454 characterization of a novel metallo-β-lactamase, TMB-1, from an Achromobacter
455 xylosoxidans strain isolated in Tripoli, Libya. Antimicrob Agents Chemother **56:**2241-2245.

456 36. **Guo Y, Wang J, Niu G, Shui W, Sun Y, Zhou H, Zhang Y, Yang C, Lou Z, Rao Z.** 2011. A
457 structural view of the antibiotic degradation enzyme NDM-1 from a superbug. Protein Cell
458 **2:**384-394.

459 37. **Vella P, Hussein WM, Leung EWW, Clayton D, Ollis DL, Mitić N, Schenk G, McGeary RP.**
460 2011. The identification of new metallo-β-lactamase inhibitor leads from fragment-based
461 screening. Bioorg Med Chem Lett **21:**3282-3285.

462 38. **Davey MS, Tyrrell JM, Howe RA, Walsh TR, Moser B, Toleman MA, Eberl M.** 2011. A
463 promising target for treatment of multidrug-resistant bacterial infections. Antimicrob Agents
464 Chemother **55:**3635-3636.

465 39. **Concha NO, Janson CA, Rowling P, Pearson S, Cheever CA, Clarke BP, Lewis C, Galleni M,**
466 **Frère JM, Payne DJ, Bateson JH, Abdel-Meguid SS.** 2000. Crystal structure of the IMP-1
467 metallo β-lactamase from Pseudomonas aeruginosa and its complex with a
468 mercaptocarboxylate inhibitor: binding determinants of a potent, broad-spectrum inhibitor.
469 Biochemistry **39:**4288-4298.

470 40. **Davies AM, Rasia RM, Vila AJ, Sutton BJ, Fabiane SM.** 2005. Effect of pH on the active site of
471 an Arg121Cys mutant of the metallo-β-lactamase from Bacillus cereus: implications for the
472 enzyme mechanism. Biochemistry **44:**4841-4849.

473 41. **Galleni M, Lamotte-Brasseur J, Rossolini GM, Spencer J, Dideberg O, Frere JM.** 2001.
474 Standard numbering scheme for class B β-lactamases. Antimicrob Agents Chemother
475 **45:**660-663.

476 42. **Brem J, Struwe WB, Rydzik AM, Tarhonskaya H, Pfeffer I, Flashman E, van Berkel SS,**
477 **Spencer J, Claridge TD, McDonough MA, Benesch JL, Schofield CJ.** 2015. Studying the active-
478 site loop movement of the Sao Paolo metallo-β-lactamase-1. Chem Sci **6:**956-963.

479 43. **Garau G, Garcia-Saez I, Bebrone C, Anne C, Mercuri P, Galleni M, Frere JM, Dideberg O.**
480 2004. Update of the standard numbering scheme for class B β-lactamases. Antimicrob
481 Agents Chemother **48:**2347-2349.

482 44. **Garcia-Saez I, Docquier JD, Rossolini GM, Dideberg O.** 2008. The three-dimensional
483 structure of VIM-2, a Zn-β-lactamase from Pseudomonas aeruginosa in its reduced and
484 oxidised form. J Mol Biol **375:**604-611.

485 45. **Zhang H, Hao Q.** 2011. Crystal structure of NDM-1 reveals a common β-lactam hydrolysis
486 mechanism. Faseb j **25:**2574-2582.

487 46. **Merino M, Perez-Llarena FJ, Kerff F, Poza M, Mallo S, Rumbo-Feal S, Beceiro A, Juan C,**
488 **Oliver A, Bou G.** 2010. Role of changes in the L3 loop of the active site in the evolution of
489 enzymatic activity of VIM-type metallo-β-lactamases. J Antimicrob Chemother **65:**1950-
490 1954.

491 47. **Mojica MF, Mahler SG, Bethel CR, Taracila MA, Kosmopoulou M, Papp-Wallace KM, Llarrull**
492 **LI, Wilson BM, Marshall SH, Wallace CJ, Villegas MV, Harris ME, Vila AJ, Spencer J, Bonomo**
493 **RA.** 2015. Exploring the Role of Residue 228 in Substrate and Inhibitor Recognition by VIM
494 Metallo-β-lactamases. Biochemistry **54:**3183-3196.

495 48. **Cadag E, Vitalis E, Lennox KP, Zhou CL, Zemla AT.** 2012. Computational analysis of
496 pathogen-borne metallo β-lactamases reveals discriminating structural features between B1
497 types. BMC Res Notes **5:**96.

498 49. **Edelstein MV, Skleenova EN, Shevchenko OV, D'Souza J W, Tapalski DV, Azizov IS,**
499 **Sukhorukova MV, Pavlukov RA, Kozlov RS, Toleman MA, Walsh TR.** 2013. Spread of

Antimicrobial Agents and Chemotherapy

500 extensively resistant VIM-2-positive ST235 Pseudomonas aeruginosa in Belarus, Kazakhstan,
501 and Russia: a longitudinal epidemiological and clinical study. Lancet Infect Dis **13:**867-876.
502 50. **Meini MR, Llarrull LI, Vila AJ.** 2015. Overcoming differences: The catalytic mechanism of
503 metallo-β-lactamases. FEBS Lett doi:10.1016/j.febslet.2015.08.015.
504

Antimicrobial Agents and Chemotherapy

505 **Table 1.** IC_{50} values for the four captopril stereoisomers and the derivatives of captopril (MBP) against different
506 MBLs. The IC_{50} values are reported in μM.

Entry	BcII	IMP-1	VIM-2	SPM-1	NDM-1
D-captopril	10.7±1.2 (45[a])	7.2±1.2	0.072±0.01	261.8±1.3	20.1±1.5(7.9[b])
L-captopril	80.4±1.1 (65[a])	23.3±1.3(12.5[a])	4.4±0.8	>500	157.4±1.3(202[b])
epi-D-captopril	>500	173.2±1.2	5.5±0.7	>500	64.6±1.4
epi-L-captopril	423.8±1.5	436±1.1	5.5±1.5	>500	>500
D-MBP	>500	>500	>500	>500	>500
L-MBP	>500	>500	>500	>500	>500

507 [a] K_i values from the literature;[b] IC_{50} values from the literature. All experiments were performed in triplicate or
508 more. Nonlinear regression analysis was used to calculate the IC_{50} values and their corresponding 95%
509 confidence intervals (GraphPad Prism). Error bars represent standard deviations.

510

511 **Table 2**. Minimum inhibitory concentrations (MICs) of meropenem (MEM) or ceftazidime (CFZ) with and

512 without D- and L-captopril (D- or L-CAP) versus various Gram negative bacteria.

Strain / Inhibitor	Genotype	MEM MIC	MEM MIC + D-CAP (8mg/L)	MEM MIC + L -CAP (8mg/L)	CFZ MIC	CFZ MIC + D-Cap (8mg/L)	CFZ MIC + L-CAP (8mg/L)
E. coli 25922	-	<0.125	<0.125	<0.125	0.125	<0.125	<0.125
E. coli J53 + NDM-1 clone	bla_{NDM-1}	64	8	8	512	8	32
E. coli J53 + NDM-1 transconjugate	bla_{NDM-1}	128	16	16	512	16	32
E. coli J53 + VIM-2 clone	bla_{VIM-2}	8	2	4	32	8	16
E. coli J53 + VIM-2 transconjugate	bla_{VIM-2}	2	1	1	32	4	8
E. coli J53 + IMP-1 clone	bla_{IMP-1}	1	0.25	0.5	128	32	32
K. pneumoniae IR16 (NDM-1)	bla_{DHA-1}, bla_{CTX-15}, bla_{TEM-1}, bla_{SHV-1}, bla_{NDM-1}	128	8	128	-	-	-
E. coli IR10 (NDM-1)	bla_{DHA-1}, bla_{CTX-15}, bla_{TEM-1}, bla_{OXA-1}, bla_{NDM-1}	64	2	64	-	-	-

K. pneumoniae IR8 (NDM-1)	*bla*$_{DHA-1}$, *bla*$_{CTX-15}$, *bla*$_{TEM-1}$, *bla*$_{SHV-1}$, *bla*$_{NDM-1}$	16	2	16	-	-	-
E. coli IR15 (NDM-1)	*bla*$_{DHA-1}$, *bla*$_{CTX-15}$, *bla*$_{TEM-1}$, *bla*$_{OXA-1}$, *bla*$_{NDM-1}$	8	0.25	8	-	-	-
K. pneumoniae IR19 (NDM-1)	*bla*$_{DHA-1}$, *bla*$_{CTX-15}$, *bla*$_{TEM-1}$, *bla*$_{SHV-1}$, *bla*$_{NDM-1}$	8	1	8	-	-	-
E. coli IR24 (NDM-1)	*bla*$_{DHA-1}$, *bla*$_{CTX-15}$, *bla*$_{TEM-1}$, *bla*$_{OXA-1}$, *bla*$_{NDM-1}$	512	32	512	-	-	
E. coli IR60 (NDM-1)	*bla*$_{DHA-1}$, *bla*$_{CTX-15}$, *bla*$_{TEM-1}$, *bla*$_{OXA-1}$, *bla*$_{NDM-1}$	128	32	128	-	-	
K. pneumoniae HR8 (NDM-1)	*bla*$_{DHA-1}$, *bla*$_{CTX-15}$, *bla*$_{TEM-1}$, *bla*$_{OXA-1}$, *bla*$_{SHV-1}$, *bla*$_{NDM-1}$	64	4	64	-	-	
K. pneumoniae N16 (NDM-1)	*bla*$_{DHA-1}$, *bla*$_{CTX-15}$, *bla*$_{TEM-1}$, *bla*$_{SHV-1}$, *bla*$_{NDM-1}$	32	4	16	-	-	
K. pneumoniae	*bla*$_{CTX-15}$, *bla*$_{TEM-}$	8	1	16	-	-	

A33 (VIM-4)	$_{1}$, *bla*$_{SHV-12a}$, *bla*$_{VIM-4}$						
K. pneumoniae A34 (VIM-4)	*bla*$_{CTX-15}$, *bla*$_{TEM-1}$, *bla*$_{SHV-12a}$, *bla*$_{VIM-4}$	8	1	8	-	-	
K. pneumoniae A35 (VIM-4)	*bla*$_{CTX-15}$, *bla*$_{TEM-1}$, *bla*$_{SHV-12a}$, *bla*$_{VIM-4}$	16	4	16	-	-	
K. pneumoniae B12 (IMP-4)	*bla*$_{CTX-15}$, *bla*$_{TEM-1}$, *bla*$_{SHV-12a}$, *bla*$_{IMP-4}$, *bla*$_{OXA-1}$	8	1	4	-	-	
S. marcescens B13 (IMP-4)	*bla*$_{DHA-1}$, *bla*$_{AMPC}$, *bla*$_{TEM-1}$, *bla*$_{IMP-4}$	4	1	4	-	-	
K. pneumoniae B19 (IMP-4)	*bla*$_{CTX-15}$, *bla*$_{TEM-1}$, *bla*$_{SHV-12a}$, *bla*$_{IMP-4}$	32	2	16	-	-	
P. aeruginosa 4470 (VIM-2)	*bla*$_{AMPC}$, *bla*$_{VIM-2}$	512	512	512			
P. aeruginosa (AIM-1)	*bla*$_{AMPC}$, *bla*$_{AIM-1}$	512	512	512			

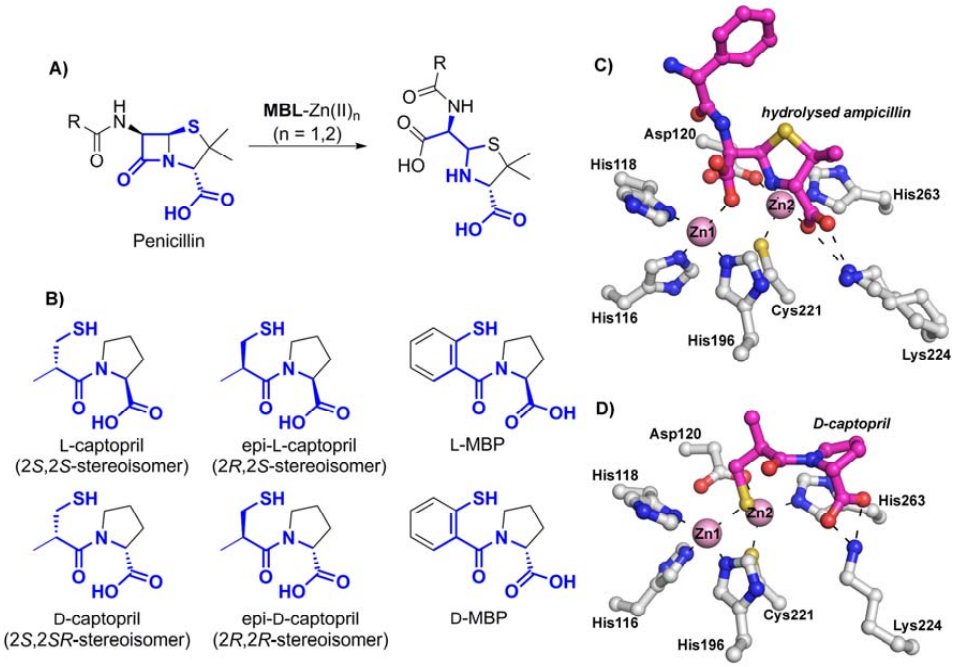

Figure 1. Captopril has structural similarity to the hydrolysed penicillin product of metallo-β-lactamase catalysis (penicilinoic acid). **A)** Outline mode of action of metallo-β-lactamases (MBLs); **B)** Structures of the 4 captopril stereoisomers (2*S*,2*S*, 2*S*,2*R*, 2*R*,2*S*, and 2*R*,2*R*), D- and L-MBP; **C**) Binding mode of hydrolysed ampicillin with NDM-1 (PDB code: 4HL2); **D**) Binding mode of D-captopril with IMP-1 (PDB ID: 4C1G – *described in this study*).

524

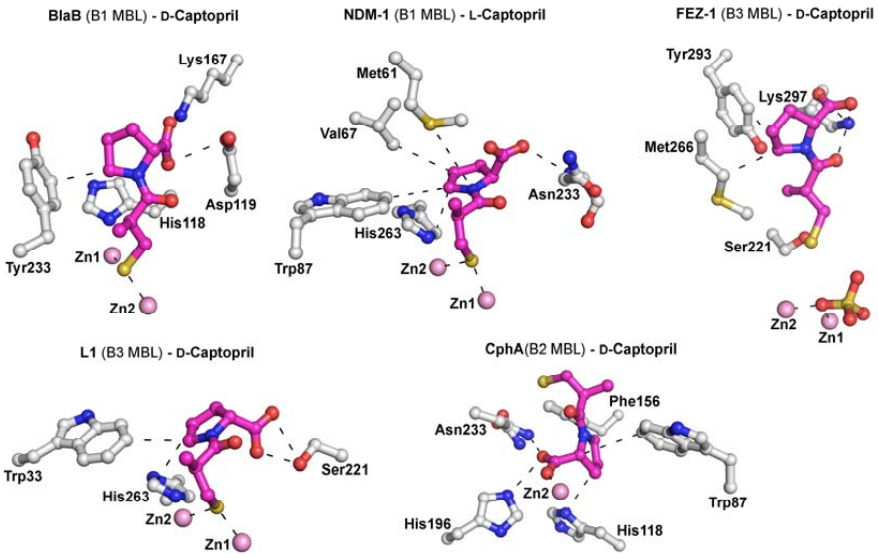

525

526 **Figure 2.** Crystallographic analysis reveal different binding modes for D- or L-captopril.
527 Preliminary crystal structures of BlaB, NDM-1, CphA, FEZ-1 and L1 complexed with L- and
528 D-captopril (PDB IDs :1M2X (1.50 Å), 4EXS (2.40 Å), 2QDS (1.66 Å), 1JT1 (1.65 Å) and
529 2FU8 (1.80 Å)). Zinc ions are represented by pink spheres, D- and L-captopril ligands are in
530 magenta, and the amino acid residues interacting with captopril are depicted as grey stick
531 models. Hydrogen bonds, zinc coordination bonds and hydrophobic interactions are shown as
532 thin black dashes.

533

534

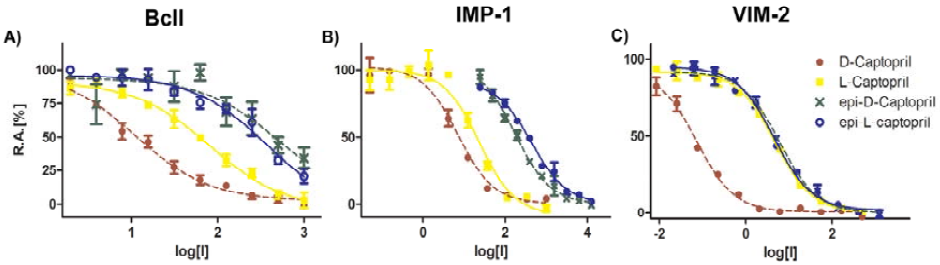

535

536 **Figure 3.** IC_{50} curves of all captopril stereoisomers tested against (**A**) BcII, (**B**) IMP-1 and

537 (**C**) VIM-2 reveal different potencies. The L- and *epi*-L-captopril stereoisomers are

538 represented with solid lines and the D- and *epi*-D-captopril stereoisomers are depicted with

539 dash lines.

540

541

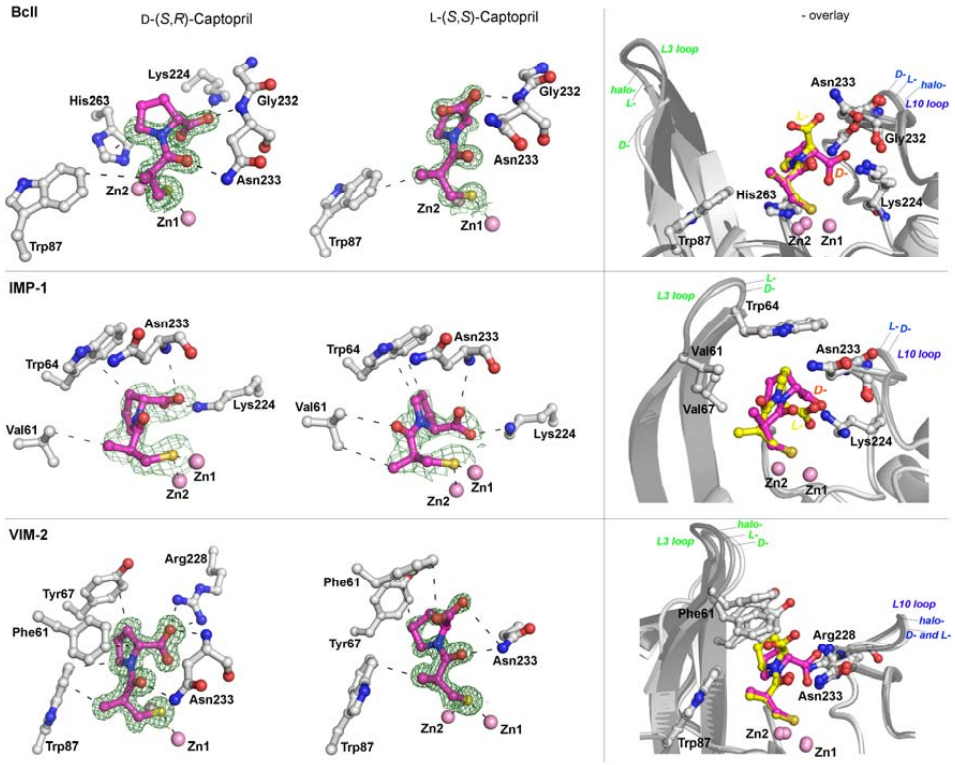

542

543 **Figure 4.** Crystallographic analyses reveal different binding modes for D- or L-captopril. The
544 left column shows views from structures of BcII, IMP-1 and VIM-2 complexed with L- and
545 D-captopril (PDB IDs: 4C1H (1.10 Å), 4C1C (1.18 Å), 4C1F (2.01 Å), 4C1G (1.71 Å), 4C1D
546 (1.20 Å) and 4C1E (1.40 Å), respectively), highlighting residues involved in inhibitor-MBL
547 complex formation. The right column shows an overlay of structures in the absence/ presence
548 of D- or L-captopril; these reveal L3 and L10 loop movements on inhibitor binding. With BcII
549 a comparison of the L3 loop was not possible, because some part of it was not modelled, but
550 clear movement was identified for the L10 loop. In the case of IMP-1 we did not obtain a di-
551 Zn(II) structure without inhibitor; a comparison with published IMP-1 structures is imprecise

552 because of different crystallisation conditions, but in the D- and L-captopril structures both L3
553 and L10 loops display different conformations. Zinc atoms are represented by pink spheres,
554 the D- and L-captopril ligands are in magenta, and the amino acid residues interacting with
555 captopril are grey stick models. The electron density maps (F_o-F_c) are contoured to 3.0 σ and
556 in green. Hydrogen bonds, zinc coordination bonds and hydrophobic interactions are thin
557 black dashes. The MBL backbone in the overlay plots is in grey and the flexible active site
558 loops are in different shades of grey (Loops L-3 and L-10)).